Available online at www.sciencedirect.com
ScienceDirect
Earth and Planetary Science Letters 249 (2006) 514–528
EPSL
www.elsevier.com/locate/epsl

The 2005, M_w 7.6 Kashmir earthquake: Sub-pixel correlation of ASTER images and seismic waveforms analysis

Jean-Philippe Avouac *, Francois Ayoub, Sebastien Leprince, Ozgun Konca, Don V. Helmberger

Tectonic Observatory, Geology and Planetary Science Division, Caltech Institute of Technology, Pasadena, CA, USA

Received 6 April 2006; received in revised form 16 June 2006; accepted 16 June 2006
Available online 17 August 2006
Editor: R.D. van der Hilst

Abstract

We analyze the M_w7.6 Kashmir earthquake of October 8, 2005, using sub-pixel correlation of ASTER images to measure ground deformation, and modeling seismic waveforms. The surface rupture is continuous over a distance of 75 km and cuts across the Hazara syntaxis reactivating the Tanda and the Muzaffarabad faults. North of Muzaffarabad the surface rupture coincides approximately with the MBT, on the southwestern flank of the syntaxis, although the two faults have opposite dip angles. The rupture terminates abruptly at the hairpin turn of the MBT showing a strong structural control. The fault offset is 4 m on average and peaks to 7 m northwest of Muzaffarabad. The rupture lasted about 25 s and propagated updip and bi-laterally by ~2 km/s, with a rise time of 2–5 s. The shallowness and compactness of the rupture, both in time and space, provide an explanation for the intensity of destructions. This kind of analysis could be achieved as soon as a post-earthquake image is available, and would provide key information for early assessment of damages. The study sheds some light on seismic hazard in the Himalaya, and raises concern regarding the possibility of a repetition of the 1555 event which presumably ruptured the Himalayan front south of the Kashmir basin and may have reached a magnitude $M_w > 8$.

Keywords: Himalaya; Kashmir Earthquakes; coseismic deformation

1. Introduction

The M_w 7.6 earthquake, which struck Northern Pakistan and Kashmir on October 8, 2005, claimed a minimum of 80,000 lives. This is to date the most devastating earthquake to have occurred along the Himalayan arc. Some earthquakes in the 20th century have probably approached or exceeded M_w 8, in particular the 1934 Bihar–Nepal and the 1905 Kangra earthquakes [1], but they did not cause as many casualties as the 2005 event (Fig. 1). This is a sad reminder that seismic vulnerability has risen critically over the last few decades due to the growth of the population in the region and probably insufficient awareness of seismic hazard [2,3].

Here, we report investigations of ground deformation in the epicentral area using optical images and measure the fault rupture by combining this information with an inversion of teleseismic body waves. Our analysis of

* Corresponding author. Tel.: +1 626 395 4239; fax: +1 626 395 1740.
E-mail address: avouac@gps.caltech.edu (J.-P. Avouac).

0012-821X/$ - see front matter © 2006 Elsevier B.V. All rights reserved.
doi:10.1016/j.epsl.2006.06.025

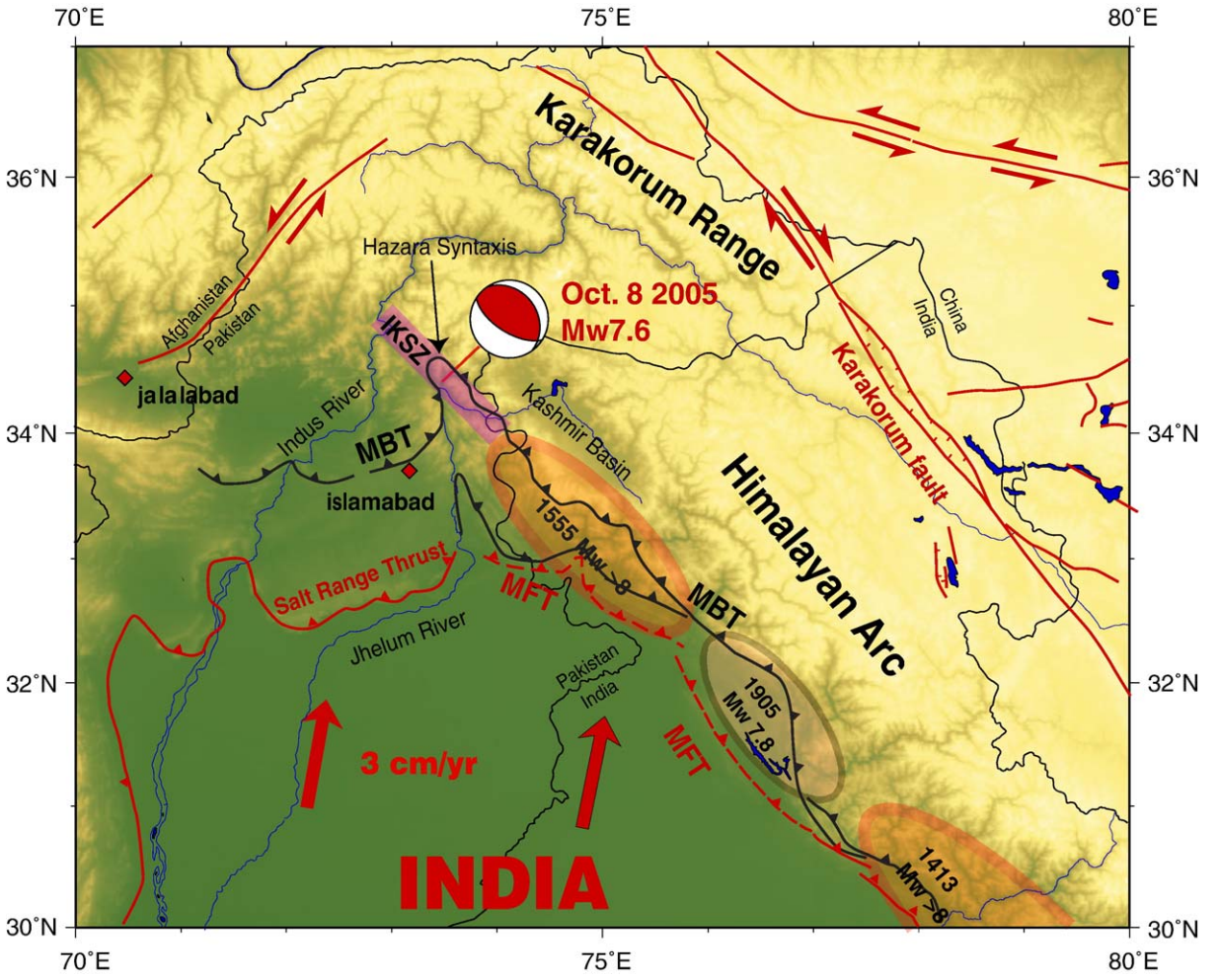

Fig. 1. Tectonic setting of the October 8, 2005, Kashmir earthquake. Rupture areas of major Himalayan earthquakes documented from historical studies [1] and paleoseismic investigations [24]. Shaded ellipses show estimated locations of ruptures in 1413, 1555 and 1905. Major active faults, modified from [52] and [24], are shown in red. Dashed lines indicate approximate location of blind thrust faults. Velocity of peninsular India relative to stable Eurasia computed from the Euler pole of the Indian plate determined by Bettinelli et al. [18]. MFT: main frontal thrust fault. MBT: main boundary thrust fault. IKSZ: Indus–Kohistan Seismic Zone [21].

this particular event brings important information on the characteristics of Himalayan earthquakes, sheds some light on the active tectonics of the western syntaxis, and opens the way to a new approach for early assessment of damages.

2. Remote sensing analysis

We measured ground deformation in the epicentral area from the sub-pixel correlation of ASTER images acquired on November 14, 2000, and October 27, 2005 (Fig. 2). We use a new procedure [4] adapted from a previous approach that had been designed specifically for processing SPOT images [5] and which has been applied to a few events [6–10]. A similar approach has been recently applied to ASTER images on the Kokoxili earthquake, yielding mitigated results [11].

The images are orthorectified on a common 15-m resolution grid using a DEM computed from a stereo pair of ASTER images. Offsets are then measured from the local cross-correlation of the two orthorectified images. Uncertainties on the imaging system, in particular on the satellite orbit and attitude, and on the topography can lead to apparent offsets unrelated to ground deformation. The satellite viewing parameters are optimized to minimize these artifacts. This process partially removes the deformation at long wavelengths, which trades off with satellite viewing

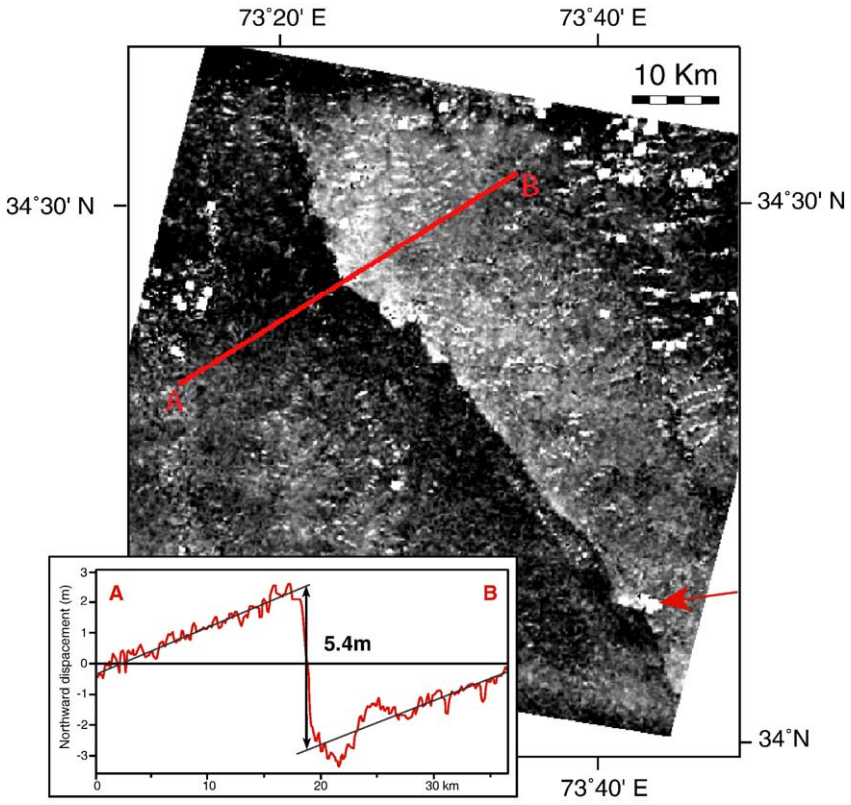

Fig. 2. Displacements measured sub-pixel correlation of ASTER images. Northward ground displacements (white to the south, black to the north), determined from the correlation of ASTER images, with a 15-m ground resolution, taken on November 14, 2000 (AST_L1A.003:2003527667) and October 27, 2005 (AST_L1A.003:2031572195). The incidence view is 8.6° for both images. The correlation image was obtained with a sliding 32×32 pixels correlation window and 8-pixel step. Ground resolution on the correlation image is 120 m. No measurement is assigned to white points, where the correlation is lost or where outliers (where the measured ground displacement was found to exceed 10 m) have been filtered out. Correlation is lost mainly due to landslides or variation of the snow cover. For example, the red arrow points to an area where the correlation is lost due a major landslide. Outliers are mostly due to shadowing effects. Inset: profile of the NS component of ground displacement obtained by stacking all measurements within a 9-km-wide swath centered on profile AB.

parameters, but significantly enhances the performance of the sub-pixel correlation technique for the measurements of deformation at short wavelengths [4]. The resulting offset field is therefore a reliable measurement of ground displacement at shorter wavelengths (typically a few kilometers).

Our measurements reveal a clear discontinuity which can be traced over a distance of about 75 km in the offset field both on the north–south (Fig. 2) and east–west (Fig. 3) components. Despite the 5-yr interval between the two images, the correlation is good, except at locations where major landslides were triggered by the earthquake (Fig. 4). We analyzed a second pair of ASTER images to evaluate the possible continuation of the rupture to the southeast. The fault trace cannot be traced beyond the area covered by the first pair of images (Fig. S1).

The horizontal slip vector on the fault can be measured accurately from profiles run across the fault trace (Fig. 2). The discontinuity is sharp, with deformation localized within a zone no wider than a few hundred meters. It clearly indicates that the rupture reached the surface, as confirmed by field investigation [12] (see also http://www.geo.oregonstate.edu/people/faculty/yeatsr.htm, Paul Tapponnier, personal communication) and inspection of high resolution optical images (Laurent Bollinger personal communication). Along the northern termination of the rupture, near Balakot, field investigations have revealed a fold scarp rather than clear ground ruptures [12]. The displacement field measured from our technique shows a rather clear discontinuity in this area suggesting that, even there, the rupture must have reached very close to the surface.

Along the upper Jhelum valley the fault trace is remarkably linear and follows the northeastern flank of the valley for about 30 km north of Muzaffarabad along

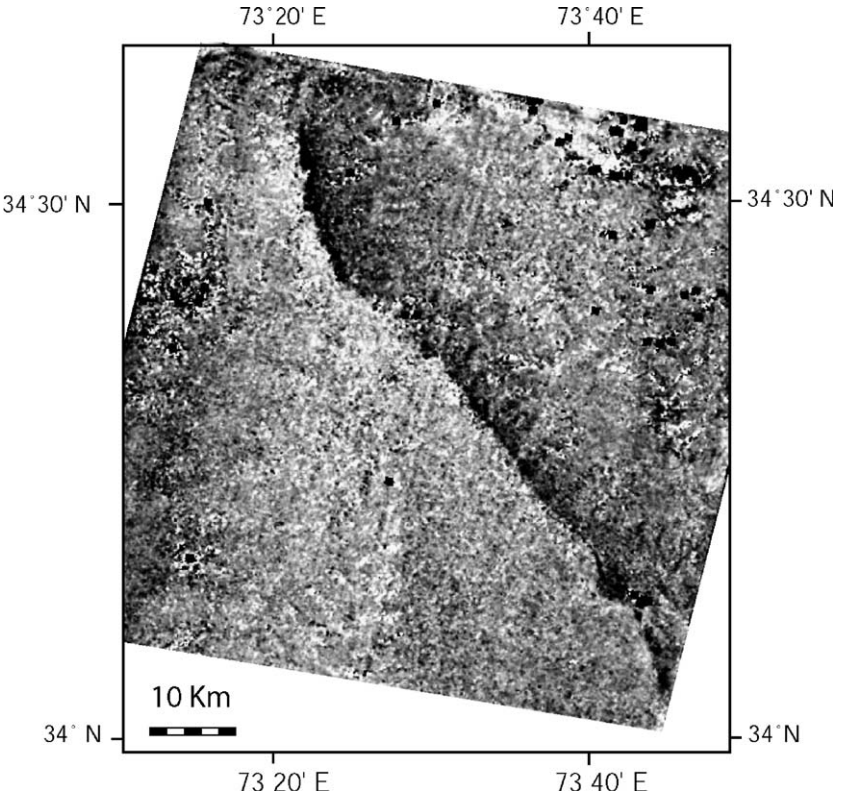

Fig. 3. EW ground displacements measured sub-pixel correlation of ASTER images. E–W ground displacements (white to the east, black to the west), determined from the correlation of ASTER images taken on November 14, 2000, and October 27, 2005. The image was obtained with a 32×32 correlation window and 8 pixel step.

the previously mapped Tanda fault [13] (Fig. 5). The fault trace curves and becomes more irregular where it joins the Muzaffarabad fault and cuts across the Kunhar valley. The irregularity of the fault trace to the north is mainly due to the roughness of the topography. The spatial variation of intersection of the fault trace with the topography shows a northeast dip angle. The fault trace makes a 'v' where it cuts across a topographic ridge south-east of the upper Jhelum river valley (box in Fig. 5). From this geometry the near surface dip angle is inferred to be about 10°. The fault's complexity across the Neelum river valley probably corresponds to a tear fault connecting the Muzaffarabad and the Tanda faults.

Horizontal slip vectors were determined about every 2 km along the fault trace from the discontinuity of ground displacement measured along profiles run across the fault (Fig. 6). The amplitude of the horizontal slip vector reaches a maximum of 7.15±0.4 m about 10 km northwest of Muzaffarabad (Fig. 6). We observe a local minimum at the junction between the Tanda and the Muzaffarabad faults. Surface slip varies quite significantly along the Muzaffarabad fault and tapers abruptly at the northern end of the rupture with a steep gradient of about 1 m/km over a distance of about 5 km. Along the straight fault segment of the Tanda Fault the horizontal slip is nearly constant, around 4±0.8 m. As the rupture approaches its crossing of the Upper Jhelum river, slip diminishes to just 1.5 m, again at a rate of about 1 m/km. In the hills further south, slip magnitude rises as high as 3.5 m, but has much more variability. The rupture is nearly pure dip–slip as the azimuth of horizontal slip motion is on average N41°E, nearly perpendicular to the 138°E average strike of the fault trace.

3. Seismological analysis

The Harvard CMT solution, determined from the modeling of the long-period surface waves, yields a northeast-dipping fault plane striking N133°E, with a rake of 123°, and a dip angle of 40° (http://www.seismology.harvard.edu/CMTsearch) (Fig. 5). The corresponding seismic moment is 2.94×10^{20} N m. Given the relatively shallow hypocentral depth, the dip angle is not well constrained from the long-period surface waves. For comparison, the focal mechanism determined by the USGS from body waves indicates a fault

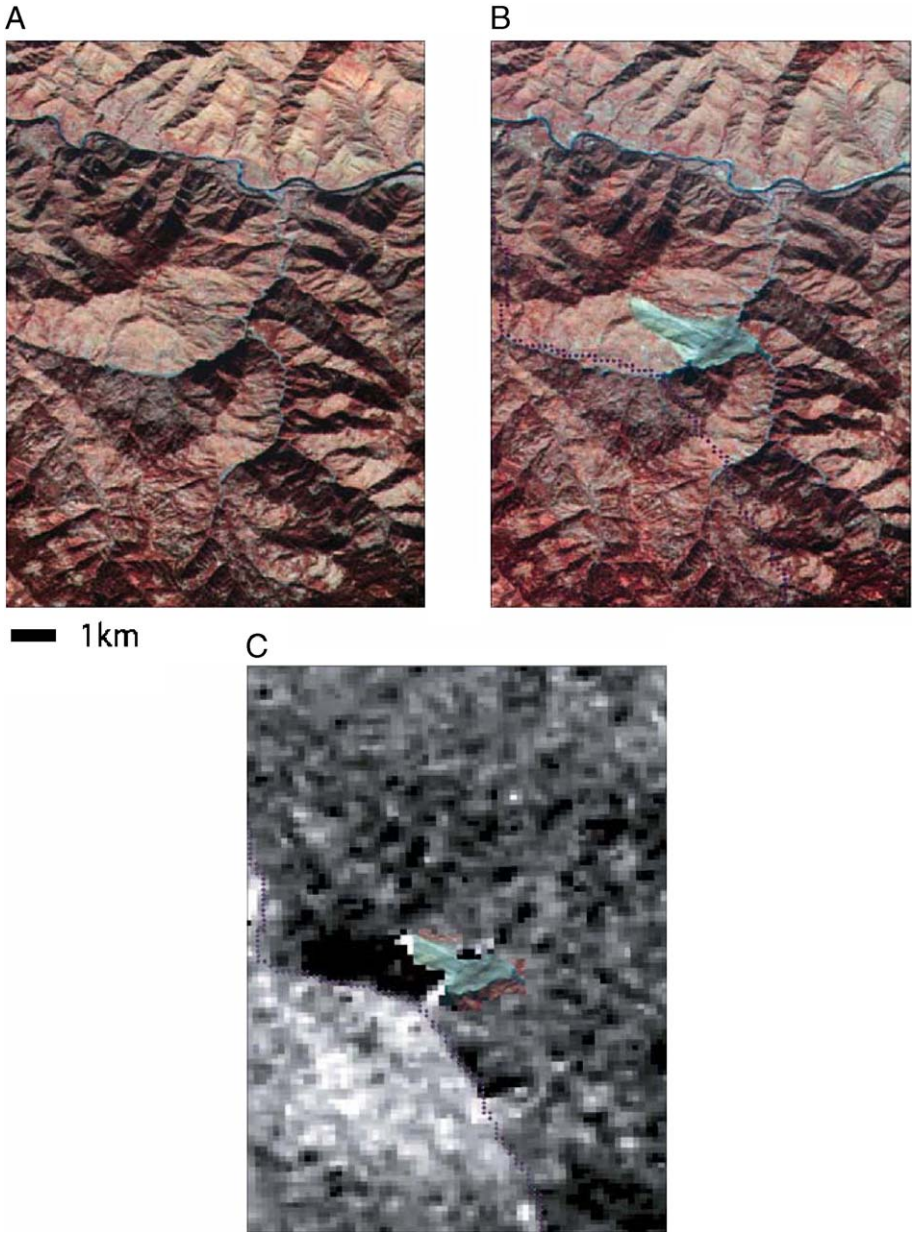

Fig. 4. Example of decorrelation due to landsliding. Close-up view of a landslide area on the ASTER image taken on November 14, 2000 (a), and October 27, 2005 (b). See Figs. 2 and 5 for location. The landslide shows up in green in (b) and corresponds closely to the area where correlation is lost. Other ASTER views of this landslide processed by Eric Fielding are accessible at http://earthobservatory.nasa.gov/NaturalHazards/, and field pictures by Bob Yeats at http://www.geo.oregonstate.edu/people/faculty/yeatsr.htm. Blue dots follow the fault trace mapped from the discontinuity in the offset field.

strike of 133°E, a rake of 140°, and a dip angle of 29° (http://neic.usgs.gov). These source parameters are consistent with the N138° fault strike determined in our study and imply a somewhat larger strike–slip component of slip than the surface slip vectors determined from the remote sensing analysis. A finite source model has also been obtained from the inversion of the teleseismic body waves by Parsons et al. [14]. This model assumes a single planar fault segment striking 108°E and dipping 31° to the northeast and a nucleation point at the USG epicenter. The model shows two distinct asperities about 30 km apart, with the nucleation point in between, and at depth shallower than about 10 km. Our measurements suggest a different fault

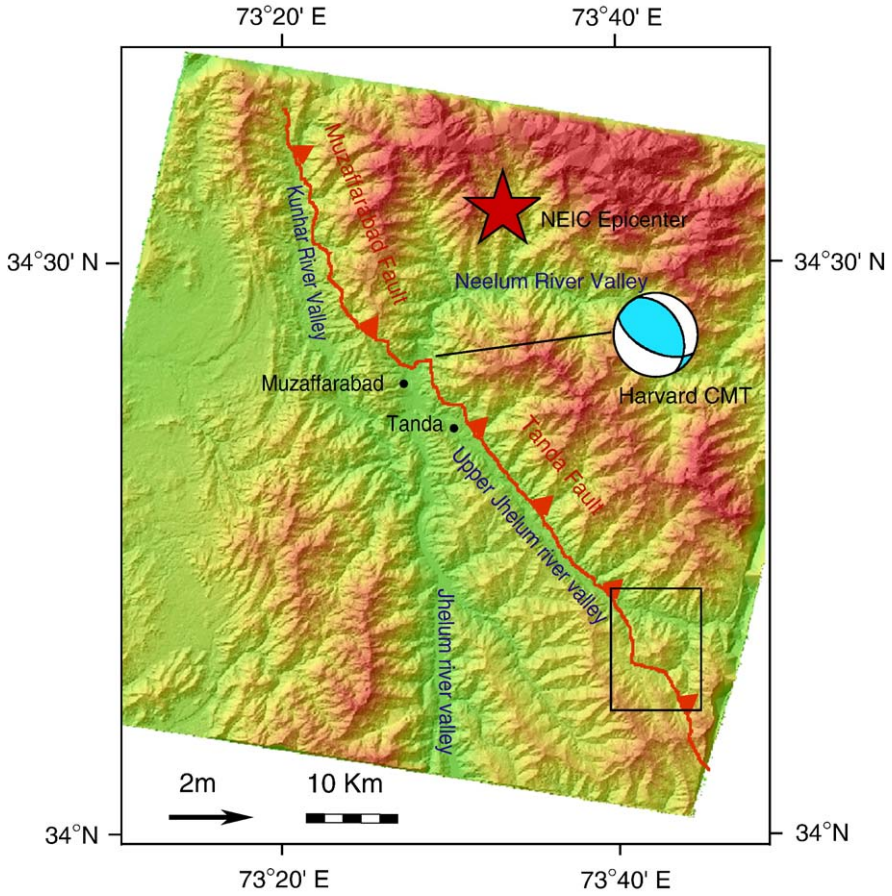

Fig. 5. Surface fault trace mapped from the discontinuity of the offset field (Figs. 3 and 4). The rupture geometry across the Neelum River and south of the Jhelum River valley (box) indicates a shallow, ~10°, dip angle near the surface.

geometry and the slip distribution at the surface does not really show two distinct asperities.

We have determined a finite source model from the modeling of teleseismic waveforms, in the 0.01–1 Hz frequency band, following the procedure of Ji et al. [15]. Fault geometry with two fault segments, a 60-km-long southern segment striking 320°, and a 15-km-long northern segment striking 343°, was constructed based on the observed surface break derived from our remote sensing analysis. These two segments approximately coincide with the Tanda and the Muzaffarabad faults, respectively. The slip vectors on the subfaults closest to the surface were constrained to fit the surface slip measurements to within $2-\sigma$. We thus assume that all of the measured slip at the surface occurred during the seismic phase, ignoring the possibility that some of it would be due to shallow afterslip over the first 3 weeks following the earthquake. In the absence of near-fault continuous geodetic measurements, we cannot test this hypothesis. We selected a set of P-wave records providing the best possible coverage in azimuth and distance (Fig. 7). We tested various dip angles between 25° and 40° and found that the polarity of the P and S wave first motions were best adjusted with a dip angle of 29°, consistent with the USGS determination. We used the USGS epicenter, which is accurate to about 20 km, to estimate the rupture initiation depth. Given the fault geometry, as defined from the fault trace at the surface and the best fitting dip angle, this assumption implies a hypocentral depth of 11 km. The best fitting model shows a simple source with a relatively compact high-slip zone spanning the Tanda and Muzaffarabad faults and mostly updip of the nucleation point (Fig. 8). The preferred model has a nearly constant rupture velocity of about 2 km/s and a short rise time between 2 s and 5 s (Fig. 7). Forcing rise times to be longer than 5 s degrades the solution (the misfit to the waveforms increases from 17.5% to 20.8%), despite the trade-off with rupture velocity. The focal mechanism representation of our finite source model is close to the Harvard CMT (Fig.

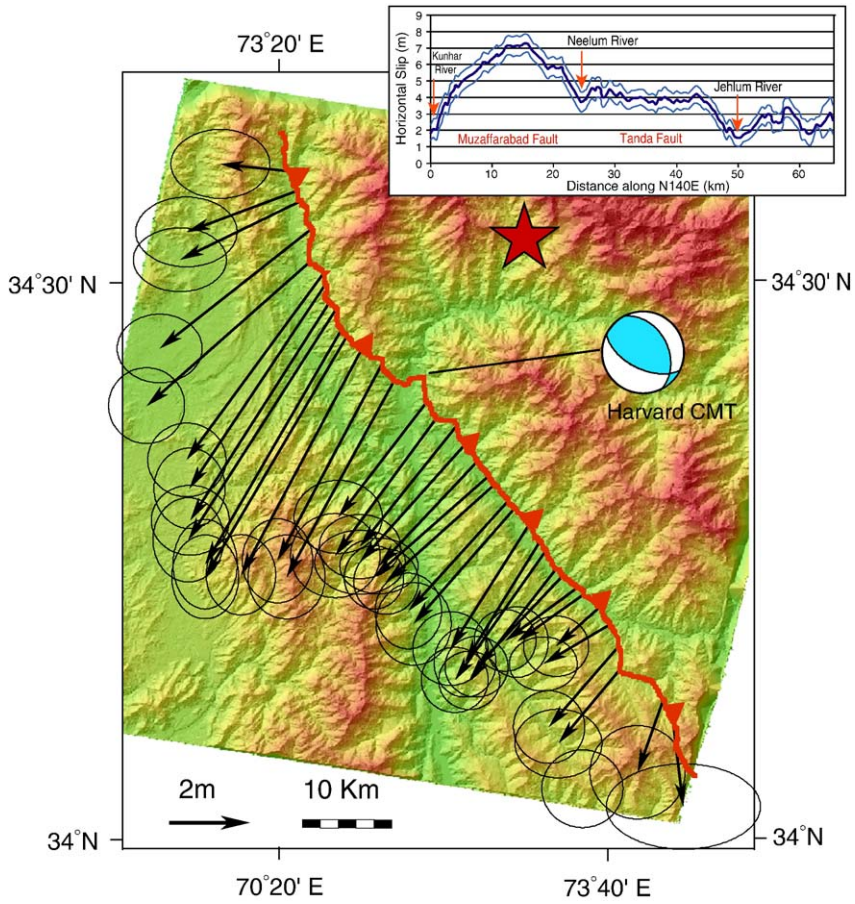

Fig. 6. Surface fault slip. Horizontal slip vectors at about 2 km spacing along the fault trace, measured from the discontinuity of E–W and N–S ground displacement measured at the fault on 18-km-long, 6-km-wide profiles run perpendicular to the fault. NS and EW offsets at the fault are measured from linear least-squares adjustment on each side of the fault. Ellipses show $2-\sigma$ uncertainties on each measurement. Inset: surface fault slip and $1-\sigma$ uncertainty projected along N140°E. Each measurement is determined from the offset at the fault of the N–S and E–W component of the offset field measured along 18-km-long and 6-km-wide profiles.

8), and the released moment is 2.82×10^{20} N m, only 4% smaller. This shows that our source model is consistent with the source model derived from the surface waves.

We have also determined a source model by inverting the teleseismic waveforms only, i.e., without any constraints on surface slip, but with the fault geometry derived from the surface fault trace. The solution is similar to that obtained form the joint inversion, showing a higher amplitude strong asperity roughly at the same location (Fig. 9). This source model yields a moment release that underestimates the Harvard CMT solution by 12%, and the misfit to the seismic waveforms is equivalent (17.8%) to that obtained from the model ignoring the constraints on surface slip. The predicted surface slip vectors systematically underestimate the measurements. Therefore, shallow slip is clearly underestimated in this model. The main reason is that the seismological waveforms are not very sensitive to slip at shallow depth (less than 2–3 km), where the elastic moduli are assumed low, because it does not contribute much to the seismic moment release. The slip distribution at shallow depth in the joint inversion is thus highly constrained by the surface measurements, while the slip distribution at depth more than about 5 km is constrained primarily by the seismic data. The slip distribution obtained from the joint inversion shows a good consistency between the slip distribution at depth and near the surface, except along the northern fault portion where the quite shallow slip is required only to fit surface fault slip.

We have also tested the sensitivity of the source model to the assumed location of the epicenter. For example, we show in Fig. S2 the solution obtained by moving the nucleation point 12 km to the

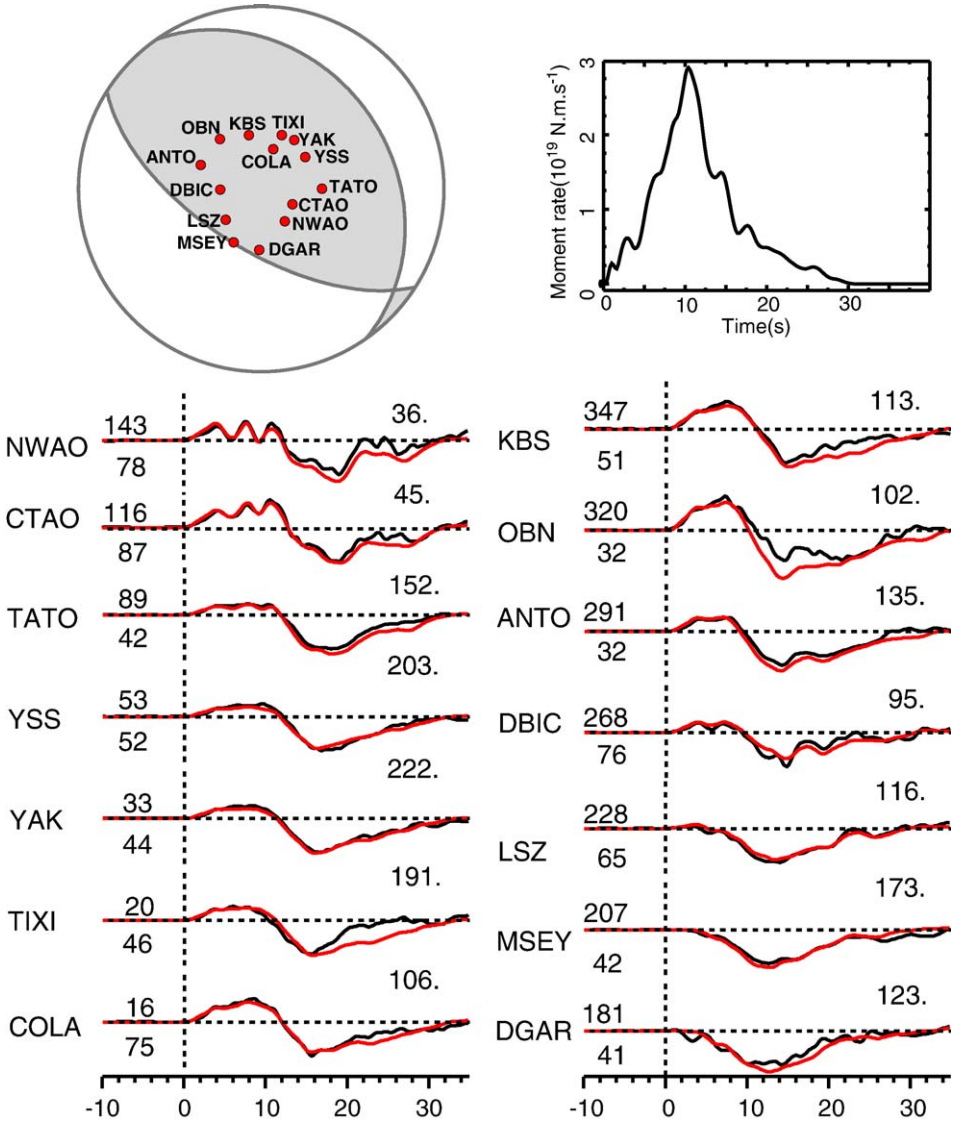

Fig. 7. Modeling of teleseismic waveforms (P waves) using the source model derived form the joint inversion of waveforms and surface slip. Measured (black) and modeled (red) seismograms. The location and the stations with respect to the focal mechanism representation of the finite source model is shown on top left. The moment release time function is shown on the top right.

northwest relative to that determined by the USGS. This particular position was tested to check the shallowness of the slip distribution along the northern portion of the fault. The solution yields about the same fit to the waveforms and surface measurements (Fig. S2). The main difference is that more slip at depth on the Muzaffarabad fault segment is now inferred. The high slip patch there, with about 14 m of slip at 5–10 km depth, is required for the seismic rupture to be still essentially bilateral, despite the position of the nucleation being close to the northern termination of the fault.

The models obtained from seismological inversion are thus quite sensitive to the assumed position of the epicenter and fault geometry. Two robust features are that the rupture was confined to relatively shallow depth, less than about 10 km, and was bilateral. It turns out that the source model obtained assuming that the USGS epicenter is correct (Fig. 4) is relatively satisfying in particular because the slip distribution is not too patchy, showing a consistent pattern near the surface, where it is constrained from our ASTER measurements, and at depth, where it is constrained from the seismic data.

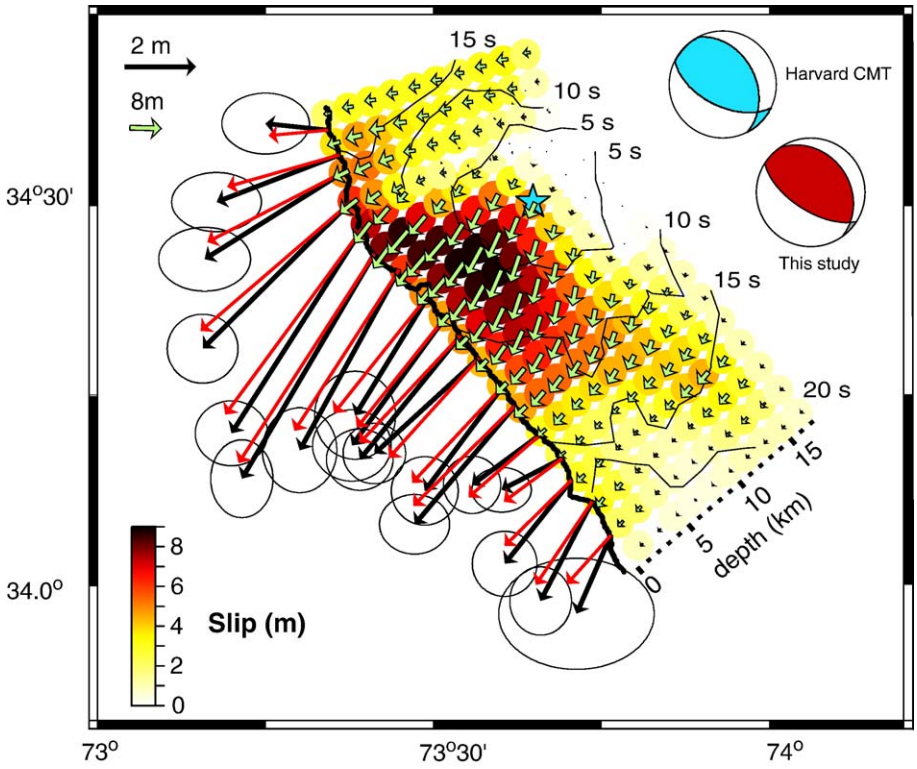

Fig. 8. Slip distribution derived from the seismic waveforms and surface slip distribution. Modeled slip distribution and isochrons showing the rupture kinematics obtained from the modeling of teleseismic body-waves. The fault geometry consists of two planar fault segments following the fault trace, subdivided in the horizontal and downdip direction in 2 km by 3 km cells. The star shows the location of the nucleation points, on the fault plane, assumed to coincide with the USGS epicenter (34.493°N,73.629°E). Seismic waveforms and surface displacements are computed in a layered half space with a 1-D crustal model interpolated from CRUST2.0 [53]. Horizontal slip vectors measured along the surface fault trace (black arrows with $2-\sigma$ uncertainty ellipses) are compared to the theoretical displacements (red arrows) computed using the method of Xie and Jao [54]. Green arrows show slip vectors on the fault plane at depth. The double-couple component of the seismic moment tensor computed from the summation of the seismic moment of each subfault of our model (red) is compared with the Harvard CMT (blue).

The source models derived from the inversion of the seismic waveforms with account for the correct location and geometry of the fault are in fact a good first order approximation. Such models would probably be enough for a reliable early assessment of near-field effects.

4. The 2005 Kashmir earthquake in its neotectonic setting

The 2005, M_w 7.6 Kashmir earthquake occurred at the western extremity of the Himalaya, where the arc joins the Karakorum, Pamir, and Hindu Kush ranges (Fig. 1). The physiography of the range, as well as geological structures define a syntaxis, called the Hazara syntaxis (or Kashmir–Hazara syntaxis), outlined by the hairpin turn of the Main Boundary thrust fault (MBT) [16]. The MBT is a major fault bounding the Himalayan range that has thrust metasediments of the Lesser Himalaya over the Tertiary molasse of the Himalayan foreland [17] (Fig. 1). Active deformation in the area results from the 31 mm/yr northward indentation of the northeastern Indian Peninsula into Eurasia [18] (Fig. 1). Along the northwestern Himalaya, a fraction of that convergence, estimated to about 14 mm/yr [19], is absorbed by thrusting perpendicular to the range.

The most active thrust fault under the Himalaya is generally thought to be the Main Frontal Himalayan Thrust fault (MFT) which marks the emergence at the surface of the Main Himalayan thrust fault (MHT), which is the basal decollement beneath the Himalayan orogenic wedge [20]. Between the Hazara syntaxis and about 76°E, the MHT is mostly blind as slip tapers below fault-tip folds [21,22]. The MHT has produced very large recurrent earthquakes with magnitudes possibly as high as M_w 8.8, as documented from paleoseismic investigations: along the Himalayan foot-

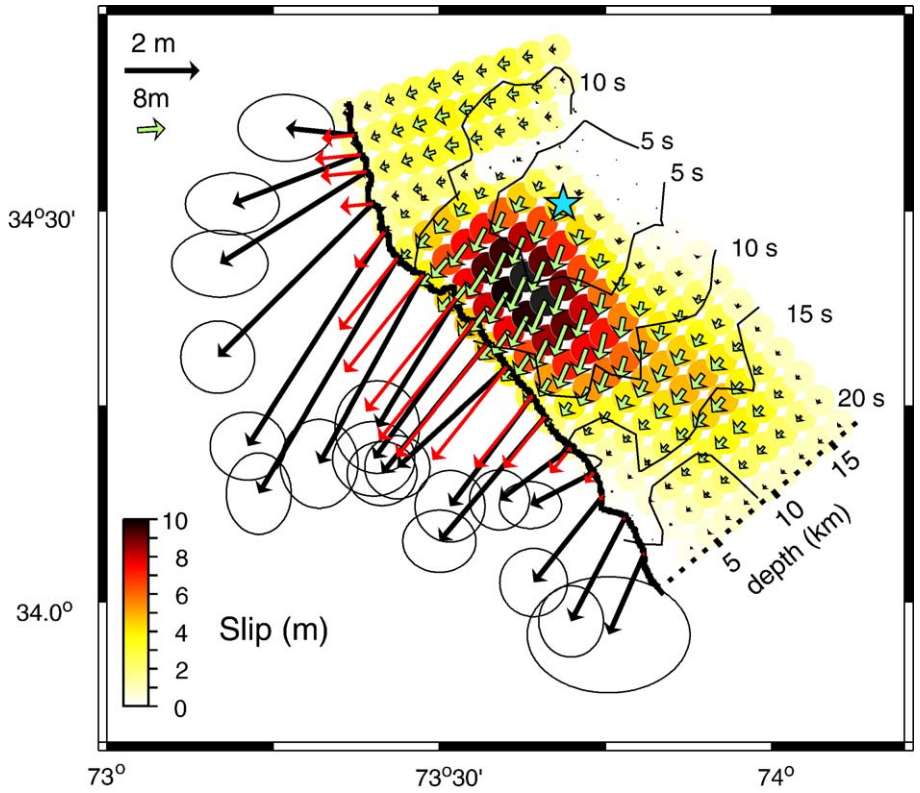

Fig. 9. Slip distribution derived from the modeling of seismic waveforms without constraints on surface slip. Modeled slip distribution and isochrons showing the rupture kinematics obtained form the modeling of teleseismic bodywaves. Horizontal slip vectors measured along the surface fault trace (black arrows with $2-\sigma$ uncertainty ellipses) are compared to the theoretical displacements (red arrows) computed using the method of Xie and Jao [54]. Green arrows show slip vectors on the fault plane at depth. The fault geometry is the same as in Fig. 3. The released moment is 2.59×10^{19} N m, about 12% less than the value associated to the Harvard CMT solution.

hills in Nepal, there is evidence for a $17+5/-3$ m slip event around 1100 AD at locations separated by 240 km along strike [23]; evidence for a similar event were also found in the Kumaon and Garhwal Himalaya and dated to around 1413 AD [24]. The loose chronological constraints are such that this rupture could correspond to the historical earthquake of 1505 AD (Tom Rockwell and Bob Yeats, personal communication) (Fig. 1).

Four major earthquakes with magnitudes close to M_w 8 occurred along the Himalaya between 1897 and 1950 [1] but none of these earthquakes was associated with a surface break. In particular, the M_w 7.8, 1905 Kangra event, which occurred along the Himalayan front southeast of Kashmir Basin and presumably ruptured the MHT but which did not reach the surface [25] (Fig. 1). The largest historical event in the northwestern Himalaya occurred in 1555 AD. Historical accounts report evidence for liquefaction and major geomorphic effects mostly in the Pir Panjal Range south of the Kashmir Basin [26] (http://asc-inia.org/gq/1555kashmir). This event may have ruptured some of the active faults mapped within the Kashmir basin itself [22] but rupture of the decollement beneath the Basin and the Pir Panjal Range seems more plausible to us. The magnitude of that earthquake remains conjectural. Given the reported effects, which suggest that MMI intensities reached XII, and the 2-month duration over which aftershocks were felt, a magnitude larger than 8 is probable [1] (Fig. 1).

Monitoring by a local seismic network around the Hazara syntaxis has revealed an alignment of seismicity, which is called the Indus–Kohistan Seismic Zone (IKSZ, Fig. 1) [21]. The IKSZ strikes parallel to the northwestern Himalaya, but extends beyond the Hazara syntaxis. This seismicity extends northwestwards the belt of seismic activity that follows the front of the entire Himalayan arc [27,28]. This is an indication that northwest-trending Himalayan basement structures extend beyond the syntaxis and that the change in the strike of the MBT is a rather superficial feature, probably related to the infracambrian salt [21]. Along

the central Nepal Himalaya the belt of seismicity has been shown to mark the downdip end of the locked portion of the MHT where interseismic stress accumulation is highest [28,29]. It has been deduced that large earthquakes break the MHT updip of this seismic zone.

5. Discussion

5.1. Performance of the sub-pixel correlation of optical images

Despite the 5-yr time difference between the two ASTER images, their sub-pixel correlation has provided a detailed description of the surface slip distribution with an accuracy not achievable by other techniques. Near the near-fault zone, our technique performs better than SAR interferometry because the coherence of SAR is often lost due to too high strain or the effect of ground shaking, or because the fringe rate exceeds the limit of one pixel-per-fringe. Cross-correlation of SAR amplitude is an alternative approach [30] which has been successfully applied to this particular earthquake [31,32], but the accuracy is not as good as what we have obtained with optical images regarding the details of the rupture geometry and the measurement of surface slip. The correlation of SAR amplitude images does, however, provide constraints on the vertical component of displacements which are not accessible from optical images. Compared to field investigations, our technique provides the two components of horizontal surface slip, whereas the component of displacement normal to the fault trace is generally not measurable in the field, and also, it takes into account deformation off the main fault trace that is generally missed during field surveys.

5.2. Characteristics of the seismic rupture

The 2005 Kashmir earthquake appears to be a simple shallow crustal event with a relatively compact slip distribution, a standard sub-shear rupture with a rather short rise time. The updip propagation of the rupture together with its steep dip angle and shallow distribution of slip must have contributed to the heavy damages in the nearfield. This event shares some similarities with the 1999, Chichi M_w 7.6 earthquake, for which a well constrained slip model has also been obtained from the joint analysis of geodetic and seismic waves [33] and which ruptured a thrust fault along the western foothills of Taiwan in a tectonic setting very similar to that along the Himalayan front. In both cases, the rupture nucleated on the bottom edge of the asperity and was restricted at depth shallower than about 15 km on relatively steep thrust faults. The shallow depth of the slip distribution is consistent with the view that deformation becomes dominantly aseismic at depth greater than about 15 km due to the transition from stick–slip to stable frictional sliding as temperature rises above 250–300 °C [34,35]. The short rise time of just 2–5 s is also a characteristic of both the Kashmir and the Chichi events and seems typical of intracontinental events as shown from other case examples of joint inversion of seismic waveforms and geodetic data [15,36–38]. By comparison, subduction events have similar rupture velocities, but seem to be characterized by much longer rise times, and hence, produce less severe ground shaking [39]. Finally, we notice that the earthquake nucleated near the junction between the Tanda and the Muzaffarabad faults.

5.3. Relation to known active faults and geological structures

The 2005 Kashmir earthquake ruptured major faults including fault segments along the Tanda and Muzaffarabad faults which had already been identified and mapped as an active fault [13,40] (note that the whole rupture is referred to as the Balakot–Bagh fault by Parsons et al. [41] and the Geological Survey of Pakistan). Geomorphic evidence for activity of the Tanda fault are also clear (Fig. 6); well developed triangular facets bound the northeastern flank of the valley; the topography northeast of the valley is systematically higher and more rugged than on the southwestern side of the valley; rivers, in particular the Neelum River, are systematically more entrenched into the hanging wall. Evidence for recent activity along the Muzaffarabad fault is more subtle: some triangular facets are apparent on the east of the Kunhar valley (Fig. 5); also, the topography is higher on the eastern side of the Kunhar valley. This is the opposite of what one would expect given that the eastern side consists of the Murree molasse, a formation much more readily erodable than the Proterozoic metasediments on the western side of the valley. It is interesting to note that the Muzaffarabad fault which has thrust the Murree formation and underlying Precambrian limestones and shales over Proterozoic formations, parallels the MBT [42] (Fig. 10) but has the opposite sense of motion and dip. This is consistent with the observation of a recent reversal of the sense of motion on the MBT [40]. It illuminates Armbruster et al.'s [43] observations that recent deformation cuts across the syntaxis.

The fact that surface ruptures along the Muzaffarabad fault parallel the MBT and terminate abruptly at the

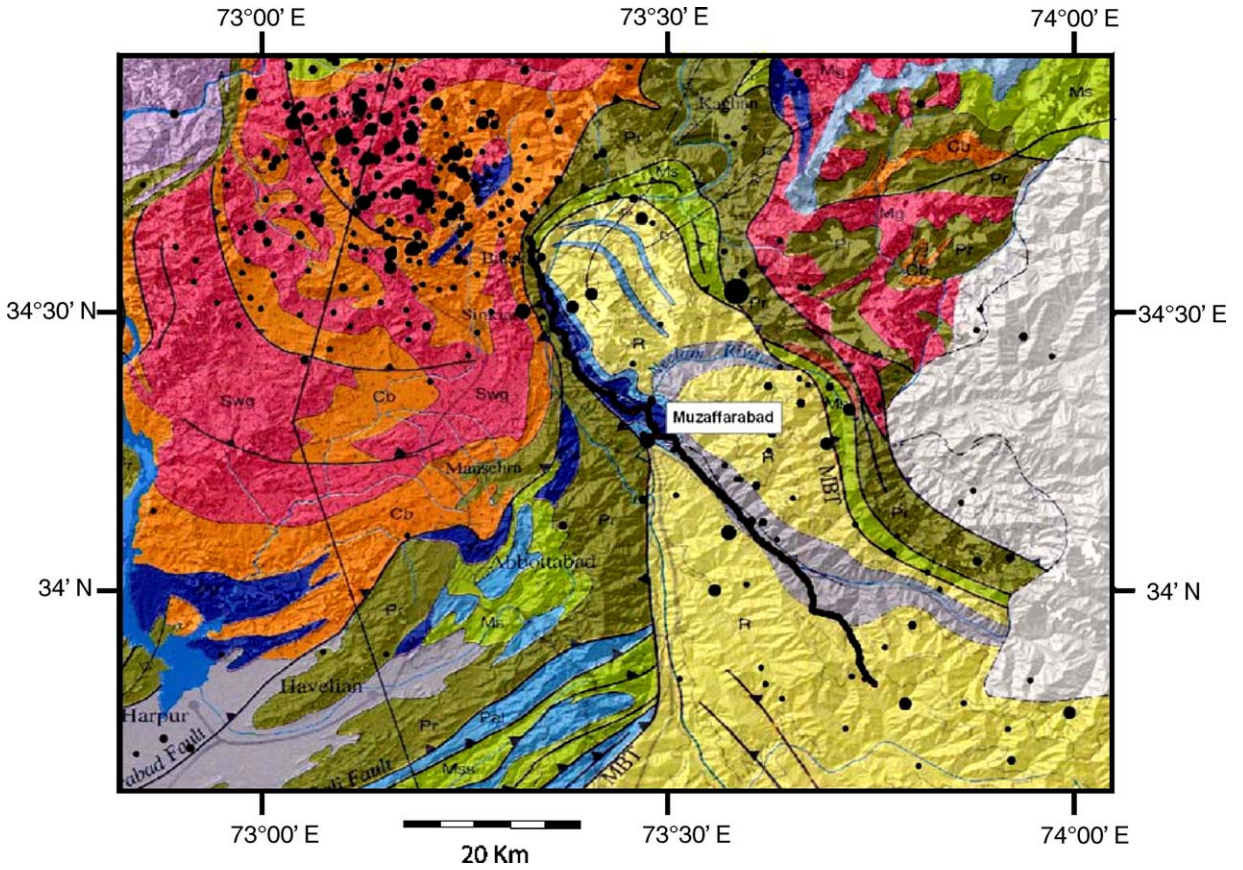

Fig. 10. Comparison of ruptured fault trace with bedrock geology. Geological map from Searle et al. [42]. Black dots show aftershocks up to December 31, 2006, with mb>4. The fault rupture coincides with the Muzaffarabad fault [40] northwest of Muzaffarabad. Southeast of Muzaffarabad, along the upper Jhelum River valley, it has reactivated the Tanda fault [13]. The fault thrusts Precambrian limestone and shales (Pz, shown in blue) over Tertiary molasse of the Murree formation (R, shown in yellow) or over Proterozoic schists (Pr, shown in green). The Muzaffarabad fault parallels the Murree thrust, which is a segment of the Main Boundary Thrust (MBT), but has as sense of motion opposite to the long-term geological motion. Southwest of Muzaffarabad the fault cuts through the Murree formation.

hairpin turn of the MBT is a clear indication for a strong structural control of the earthquake rupture. We also observe that the surface slip is relatively uniform along the straight fault segment along the Upper Jhelum river, suggesting that variability of the slip and geometric complexity are correlated and decrease with cumulative geological offset [44].

It is noteworthy that the aftershock activity does not correlate well with the extent of the surface ruptures and was particularly intense beyond the abrupt northern termination of rupture (Fig. 10), along the IKSZ.

5.4. Importance of out-of-sequence thrusting for seismic hazard along the Himalayan arc

The 2005 Kashmir earthquake might be compared to the most recent damaging earthquakes along the Himalaya, the M_s 7.1 Uttarkashi earthquake of 1991 [45] and the M_s 6.6 Chamoli earthquake of 1999 [46] which both occurred in the Garhwal Himalaya. Both earthquakes were caused by the rupture of blind thrust faults dipping about 10° to the north, probably on the deep portion of the MHT. In contrast, the Kashmir earthquake was not on the basal detachment. Instead it occurred on a relatively steep fault that splays upward from it, like probably the 1974 Pattan earthquake [47]. One might wonder whether such out-of-sequence thrust events, potentially much more damaging than the Chamoli or Uttarkashi earthquakes, should be expected elsewhere along the Himalaya. Evidence for brittle faulting along the front of the high range have been reported elsewhere, in particular in the Nepal Himalaya, showing that out-of-sequence thrusting can indeed occur [48] possibly as a response to locally enhanced erosion [49]. However, for the Nepal Himalaya, it can be argued that such out-of-sequence thrust events must be

rare. Indeed, the observation that the geological slip rate of the MFT [50] is not significantly different from the geodetic convergence rate the across central Nepal Himalaya [18] implies that most of the shortening is localized on the MHT, probably as a result of repeated $M>8$ large earthquake. Elsewhere along the arc the situation might be different. However, it might be that the particular setting of the Kashmir event near the western syntaxis makes out-of-sequence thrust events more frequent than along the main stretch of the Himalayan arc. Thrust faulting within the orogenic wedge might be the mechanism by which the wedge maintains its critical slope in response to the particularly rapid erosion rates in the Hazara syntaxis [51] and eventually to spreading of the thrust sheet due to aseismic creep along the basal detachment.

5.5. Return period of major earthquakes across the Himalaya of Kashmir and Himachal Pradesh

The average slip on the fault patch ruptured by the 2005 Kashmir earthquake is ~4.2 m. If the geodetically determined ~14 mm shortening rate across the range were accommodated by the repetition of such earthquakes, their return period along this particular segment of the arc would be about 300 yr. Given the ~600-km length of the stretch of the Himalayan arc between the Hazara syntaxis and Dehra Dun (corresponding to the area pictured in Fig. 1), the return period of such events over the whole area would be about 30 to 40 yr. The historical catalogue is well short of such events. It seems therefore likely that shortening across the northwestern Himalaya is primarily the result of less frequent but significantly larger events, the 1555 AD event being one of these.

Stress redistribution during the Kashmir event must have increased the stresses on the major thrust faults south-east of the Hazara syntaxis and therefore increased the probability of a new seismic rupture in the Himalaya of Kashmir and Himachal. By contrast this event does not seem to have increased the probability of an earthquake along the Salt Range Thrust [41], even more so if the Salt Range thrust is creeping aseismically due the Infracambrian salt layer at the base of the thrust sheet [21], but this idea remains to be tested from geodetic measurements.

6. Conclusion

The Kashmir 2005 earthquake is the first modern earthquake in the Himalaya to produce documented surface rupture. Despite the complex geological setting associated with the Hazara syntaxis, the slip pattern and source kinematics are relatively simple. This earthquake occurred along the seismicity belt which follows the front of the high range all along the arc, but it departs from previous events with similar magnitudes since it was caused by rupture of a steeply dipping thrust fault that broke all the way to the surface. The 2005 Kashmir shows that seismic hazard related to out-of-sequence thrusting in the Himalaya can be devastating and should not be overlooked, although major events along the MHT seem much more probable.

The 2005 earthquake must have increased the probability of rupture along the MHT or possible out-of-sequence thrust faults along the Himalayan front to the south east, with the possible repetition of events such the 1555 AD earthquake. The death toll in such an event would probably be even larger than in 2005. This should be a major concern for the growing population living in the region.

This study, carried on with 15-m resolution images taken 5 yr apart, demonstrates the potential of optical imagery as a complement to seismology for the analysis of large earthquakes. A global coverage already exists thanks to the SPOT and ASTER programs, and there is no doubt that high-quality optical imagery, with metric or submetric resolution, will be available in the future. This warrants that the approach described here will be applicable to future large earthquake. Well constrained source models, and some estimate of near-field effects, could be produced a couple of hours after the images are available.

Acknowledgments

This study has benefited from useful discussions with Kerry Sieh, Chen Ji, James Jackson, Eric Fielding, Mohamed Chlieh, Laurent Bollinger, Roland Burgmann. We are most grateful to Bob Yeats and Barry Parsons for helpful reviews.

Appendix A. Supplementary data

Supplementary data associated with this article can be found, in the online version, at doi:10.1016/j.epsl.2006.06.025.

References

[1] R. Bilham, Earthquakes in India and the Himalaya: tectonics, geodesy and history, Ann. Geophys. 47 (2004) 839–858.
[2] R. Bilham, V.K. Gaur, P. Molnar, Earthquakes—Himalayan seismic hazard, Science 293 (2001) 1442–1444.

[3] J. Jackson, Fatal attraction: living with earthquakes, the growth of villages into megacities, and earthquake vulnerability in the modern world, Philos. Trans. R. Soc. Lond. A 364 (2006) 1911–1925, doi:10.1098/rsta.2006.1805.
[4] S. Leprince, S. Barbot, F. Ayoub, J.P. Avouac, Automatic and precise ortho-rectification, co-registration and sub-pixel correlation of satellite images, application to ground deformation measurements, IEEE Trans. Geosci. Remote Sens. (in press).
[5] N. Van Puymbroeck, R. Michel, R. Binet, J.P. Avouac, J. Taboury, Measuring earthquakes from optical satellite images, Appl. Opt. Inf. Process. 39 (2000) 1–14.
[6] K.L. Feigl, F. Sarti, H. Vadon, P. Purand, S. Mclusky, S. Ergintav, R. Bürgmann, A. Rigo, D. Massonnet, R. Reilinger, Estimating slip distribution for the Izmit mainshock from coseismic GPS, ERS-1, RADARSAT and SPOT measurements, Bull. Seismol. Soc. Am. 92 (2002) 138–160.
[7] R. Michel, J.P. Avouac, Deformation due to the 17 August 1999 Izmit, Turkey, earthquake measured from SPOT images, J. Geophys. Res., [Solid Earth] 107 (2002) (art. no.-2062).
[8] S. Dominguez, J.P. Avouac, R. Michel, Horizontal coseismic deformation of the 1999 Chi-Chi earthquake measured from SPOT satellite images: implications for the seismic cycle along the western foothills of central Taiwan, J. Geophys. Res., [Solid Earth] 108 (2003) (art. no.-2083).
[9] R. Binet, L. Bollinger, Horizontal coseismic deformation of the 2003 Bam (Iran) earthquake measured from SPOT-5 THR satellite imagery, Geophys. Res. Lett. 32 (2005).
[10] Y. Klinger, R. Michel, G.C.P. King, Evidence for an earthquake barrier model from M_w similar to 7.8 Kokoxili (Tibet) earthquake slip-distribution, Earth Planet. Sci. Lett. 242 (2006) 354–364.
[11] C.G. Schiek, J.H. Hurtado Jr., Slip analysis of the Kokoxili earthquake using terrain-change detection and regional earthquake data, Geosphere 2 (2006) 187–194.
[12] R.S. Yeats, A. Hussain, Surface Features of the M_w 7.6, 8 October 2005 Kashmir Earthquake, Northern Himalaya, Pakistan: Implications for the Himalayan Front, SSA, San Francisco, CA, 2006.
[13] T. Nakata, H. Tsutsumi, S.H. Khan, R.D. Lawrence, Active Faults of Pakistan, Research Center for Regional Geography Hiroshima University, Hiroshima, Japan, 1991, 141 pp.
[14] T. Parsons, R.S. Yeats, Y. Yagi, A. Hussain, Static stress change from the 8 October, 2005 M=7.6 Kashmir earthquake, Geophys. Res. Lett. 33 (2006).
[15] C. Ji, D. Wald, D.V. Helmberger, Source description of the 1999 Hector Mine, California earthquake: Part I. Wavelet domain inversion theory and resolution analysis, Bull. Seismol. Soc. Am. 92 (2002) 1192–1207.
[16] P.J. Treloar, M.P. Coward, A.F. Chambers, C.N. Izatt, K.C. Jackson, Thrust geometries, interferences anti rotations in the Northwest Himalaya, in: K.R. McCiay (Ed.), Thrust Tectonics, Chapman and Halt, London, UK, 1992, pp. 325–342.
[17] A. Gansser, Geology of the Himalayas, Interscience Publishers, London, 1964, 289 pp.
[18] P. Bettinelli, J.-P. Avouac, M. Flouzat, F.O. Jouanne, L. Bollinger, P. Willis, G. Chitrakar, Plate motion of India and interseismic strain in the Nepal Himalaya from GPS and DORIS measurements, J. Geod. (2006) 1–23.
[19] P. Banerjee, R. Burgmann, Convergence across the northwest Himalaya from GPS measurements, Geophys. Res. Lett. 29 (2002) (art. no.-1652).
[20] M.L. Hauck, K.D. Nelson, L.D. Brown, W. Zhao, A.R. Ross, Crustal structure of the Himalayan orogen at 90deg east longitude from project INDEPTH deep reflection profiles, Tectonics 17 (1998) 481–500.
[21] L. Seeber, J. Armbruster, R. Quittmeyer, Seismicity and continental collision in the Himalayan arc, in: H.K. Gupta, F. M. Delany (Eds.), Zagros–Hindukush–Himalaya: Geodynamic Evolution 3, Geodynamic Series, American Geophysical Union, Washington, 1981, pp. 215–242.
[22] R.S. Yeats, T. Nakata, A. Farah, M.A. Mizra, M.R. Pandey, R.S. Stein, The Himalayan frontal fault system, in: DeJong, Farah (Eds.), Geodynamics of Pakistan, Geological Survey of Pakistan: Seismicity of the Hazara Arc in Northern Pakistan: Decollement vs. Basement Faulting, Annales Tectonicae Special Issue Supplement to Volume VI, 1992, pp. 85–98.
[23] J. Lavé, D. Yule, S. Sapkota, K. Basant, C. Madden, M. Attal, R. Pandey, Evidence for a great medieval earthquake (approximate to 1100 AD) in the Central Himalayas, Nepal, Science 307 (2005) 1302–1305.
[24] S. Kumar, S.G. Wesnousky, T.K. Rockwell, R. Briggs, V.C. Thakur, R. Jayangondaperumal, Paleoseismic evidence of great surface-rupture earthquakes along the Indian Himalaya, J. Geophys. Res. 111 (2006), doi:10.1029/2004JB003309.
[25] K. Wallace, R. Bilham, F. Blume, V.K. Gaur, V. Gahalaut, Surface deformation in the region of the 1905 Kangra M_w=7.8 earthquake in the period 1846–2001, Geophys. Res. Lett. 32 (2005).
[26] R.N. Iyengar, D. Sharma, J.M. Siddiqui, Earthquake history of India in medievel times, Indian J. Hist. Sci. 34 (1999).
[27] J. Baranowski, J. Armbruster, L. Seeber, P. Molnar, Focal depths and fault plane solutions of earthquakes and active tectonics of the Himalaya, J. Geophys. Res. 89 (1984) 6918–6928.
[28] M.R. Pandey, R.P. Tandukar, J.P. Avouac, J. Lave, J.P. Massot, Interseismic strain accumulation on the Himalayan crustal ramp (Nepal), Geophys. Res. Lett. 22 (1995) 751–754.
[29] L. Bollinger, J.P. Avouac, R. Cattin, M.R. Pandey, Stress buildup in the Himalaya, J. Geophys. Res. 109 (2004), doi:10.1029/2003JB002911.
[30] R. Michel, J.P. Avouac, J. Taboury, Measuring ground displacements from SAR amplitude images: application to the Landers earthquake, Geophys. Res. Lett. 26 (1999) 875–878.
[31] S. Fujiwara, M. Tobita, H.P. Sato, S. Ozawa, H. Une, M. Koaarai, H. Nakai, M. Fujiwara, H. Yarai, T. Nishimura, F. Hayashi, Satellite data gives snapshot of the 2005 Pakistan earthquake, EOS, Trans.-Am. Geophys. Union 87 (2006).
[32] E. Pathier, E.J. Fielding, T.J. Wright, R. Walker, B.E. Parsons, Displacement field and slip distribution of the 2005 Kashmir earthquake from SAR imagery, Geophys. Res. Lett. (submitted for publication).
[33] C. Ji, D.V. Helmberger, T.-R.A. Song, K.-F. Ma, D.J. Wald, Slip distribution and tectonic implications of the 1999 Chi-Chi, Taiwan earthquake, Geophys. Res. Lett. 28 (2001) 4379–4382.
[34] J.P. Avouac, Mountain building, erosion and the seismic cycle in the Nepal Himalaya, in: R. Dmowska (Ed.), Advances in Geophysics, vol. 46, Elsevier, Amsterdam, 2003.
[35] C. Scholz, The Mechanics of Earthquakes and Faulting, Cambridge University Press, New York, 1990, 439 pp.
[36] B. Hernandez, F. Cotton, M. Campillo, Contribution of radar interferometry to a two-step inversion of the kinematic process of the 1992 Landers earthquake, J. Geophys. Res., [Solid Earth] 104 (1999) 13083–13099.
[37] C. Ji, K.M. Larson, Y. Tan, K.W. Hudnut, K.H. Choi, Slip history of the 2003 San Simeon earthquake constrained by combining 1-

Hz GPS, strong motion, and teleseismic data, Geophys. Res. Lett. 31 (2004).
[38] B. Delouis, D. Giardini, P. Lundgren, J. Salichon, Joint inversion of InSAR, GPS, teleseismic, and strong-motion data for the spatial and temporal distribution of earthquake slip: application to the 1999 Izmit mainshock, Bull. Seismol. Soc. Am. 92 (2002) 278–299.
[39] A.O. Konca, V. Hjorleifsdottir, T.R.A. Song, J.P. Avouac, D.V. Helmberger, C. Ji, K. Sieh, R. Briggs, A. Meltzner, Rupture kinematics of the 2005, M_w 8.6, Nias-Simeulue earthquake from the joint inversion of seismic and geodetic data, Bull. Seismol. Soc. Am. (in press).
[40] J.A. Calkins, T.W. Offield, S.K.M. Abdullah, S.T. Ali, Geology of the southern Himalaya in Hazara, Pakistan and adjacent areas, U.S. Geological Survey Professional Paper, vol. 716-C, U.S. Government Printing Office, Washington, D.C., 1975.
[41] T. Parsons, R.S. Yeats, Y. Yagi, A. Hussain, Static stress change from the 8 October, 2005 M=7.6 Kashmir earthquake, Geophys. Res. Lett. 33 (2006) LO6304.
[42] M.P. Searle, M. Khan, M.Q. Jan, J.A. DiPietro, K.R. Pogue, D.A. Pivnik, W.J. Sercombe, C.N. Izatt, P.M. Blisniuk, P.J. Treloar, M. Gaetani, A. Zanchi, Geological Map of North Pakistan (Western Himalaya, Salt Ranges, Kohistan, Karakoram, Hindu Kush), 1996.
[43] J. Armbruster, L. Seeber, K.H. Jacob, Northwestern termination of Himalayan mountain front—active tectonics from micro-earthquakes, J. Geophys. Res. 83 (1978) 269–282.
[44] S.G. Wesnousky, Seismicity as a function of cumulative geologic offset: some observations from southern California, Bull. Seismol. Soc. Am. 80 (1990) 1374–1381.
[45] F. Cotton, M. Campillo, A. Deschamps, B.K. Rastogi, Rupture history and seismotectonics of the 1991 Uttarkashi, Himalaya earthquake, Tectonophysics 258 (1996) 35–51.
[46] K. Rajendran, C.P. Rajenddran, S. Jain, C.V.R. Murty, J.N. Arlekar, The Chamoli earthquake, Garhwal Himalaya: field observations and implications for seismic hazard, Curr. Sci. 78 (2000) 45–51.
[47] W.D. Pennington, A summary of field and seismic observations of the Pattan earthquake—28 December 1974, in: A. Farah, K.A. DeJong (Eds.), Geodynamics of Pakistan, Geological Survey of Pakistan, 1989, pp. 143–147.
[48] T. Nakata, Active faults of the Himalaya of India and Nepal, in: L.L. Malinconico Jr., R. Lillie (Eds.), Tectonics of the Western Himalayas Special Paper, vol. 232, Geol. Soc. of America, 1989, pp. 243–264.
[49] K.V. Hodges, C. Wobus, K. Ruhl, T. Schildgen, K. Whipple, Quaternary deformation, river steepening, and heavy precipitation at the front of the Higher Himalayan ranges, Earth Planet. Sci. Lett. 220 (2004) 379–389.
[50] J. Lavé, J.P. Avouac, Active folding of fluvial terraces across the Siwaliks Hills, Himalayas of central Nepal, J. Geophys. Res. 105 (2000) 5735–5770.
[51] P.K. Zeitler, P.O. Koons, M.P. Bishop, C.P. Chamberlain, D. Craw, M.A. Edwards, S. Hamidullah, M. Oasim Jan, M. Asif Khan, M. Umar Khan Khattak, W.S.F. Kidd, R.L. Mackie, A.S. Meltzer, S.K. Park, A. Pêcher, M.A. Poage, G. Sarker, D.A. Schneider, L. Seeber, J.F. Shroder, Crustal reworking at Nanga Parbat, Pakistan: metamorphic consequences of thermal–mechanical coupling facilitated by erosion, Tectonics 20 (2001) 712–728.
[52] R.S. Yeats, T. Nakata, A. Farah, M. Fort, M.A. Mirza, M.R. Pandey, R.S. Stein, The Himalayan frontal fault system, Ann. Tecton. 6 (1992) 85–98.
[53] C. Bassin, G. Laske, G. Masters, The current limits of resolution for surface wave tomography in North America, EOS, Trans.-Am. Geophys. Union 81 (48) (2000) S12A-03.
[54] X. Xie, Z.X. Yao, A generalized reflection-transmission coefficient matrix method to calculate static desplacement field of a dislocation source in a stratified half space, Chin. J. Geophys. 32 (1989) 191–205.